I&EC research
Industrial & Engineering Chemistry Research

Article

pubs.acs.org/IECR

Carbon Nanofiber-Based Palladium/Zinc Catalysts for the Hydrogenation of Carbon Dioxide to Methanol at Atmospheric Pressure

Javier Díez-Ramírez,* Paula Sánchez, Alberto Rodríguez-Gómez, José Luis Valverde, and Fernando Dorado

Departamento de Ingeniería Química, Facultad de Ciencias y Tecnologías Químicas, Universidad de Castilla−La Mancha, Avenida Camilo José Cela 12, 13071 Ciudad Real, Spain

ABSTRACT: Palladium/zinc catalysts supported on carbon nanofibers (CNFs) have been used to study the catalytic performance in the hydrogenation of CO_2 to obtain methanol at atmospheric pressure. The carbon nanofiber support has an influence on the nature of the PdZn alloy formed. The effect of the Pd/Zn molar ratio on the PdZn alloy particle size was analyzed. Lower Pd/Zn molar ratio leads to higher PdZn alloy particle size, which was associated with higher selectivity toward methanol. The influence of the type of nanofiber (platelet or fishbone) on the catalytic behavior was also studied and compared with that of a conventional Pd/ZnO catalyst. The palladium/zinc catalyst supported on platelet nanofiber was considered to be a good candidate for the hydrogenation of carbon dioxide to methanol.

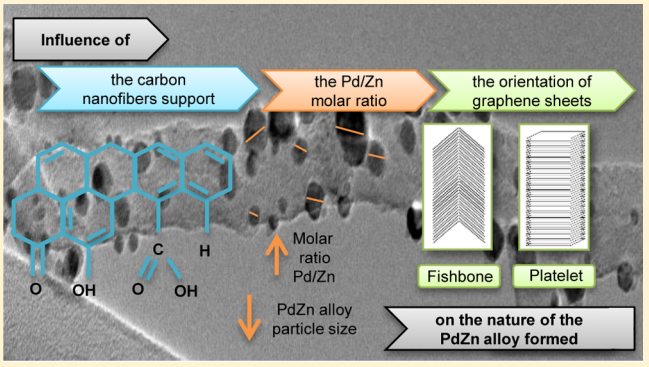

1. INTRODUCTION

World CO_2 emissions from fuel combustion increased by 51.5% from 1990 to 2012.[1] In addition, projections confirm that CO_2 emissions from the power sector will rise from 13.2 Gt (where Gt denotes gigatonnes) in 2012 to 15.4 Gt in 2040, retaining a share of ∼40% of global emissions over this period.[2] Based on this information, it is important to focus our efforts on reducing the levels of emissions. One way to mitigate the increase in CO_2 in the atmosphere is to exploit carbon dioxide to obtain products of value.

The hydrogenation of carbon dioxide has been assessed as one of the reactions to produce added-value products such as hydrocarbons or alcohols.[3] In this reaction, hydrogen attacks the nonreactive CO_2, as shown in the general reaction described in eq 1.

$$xCO_2 + \left(2x - z + \frac{y}{2}\right)H_2 \rightarrow C_xH_yO_z + (2x - z)H_2O \quad (1)$$

The use of hydrogen in this reaction limits the economy of the process; however, this aspect could be changed if the hydrogen was obtained from renewable sources.[4]

One of the most important products obtained from the aforementioned reaction is methanol (when $x = 1$, $y = 4$, and $z = 1$), as shown in eq 2.

$$CO_2 + 3H_2 \leftrightarrows CH_3OH + H_2O \qquad \Delta H_{25\,^\circ C} = -49.5\ \text{kJ/mol} \quad (2)$$

Methanol is frequently used as a solvent and a feedstock for the production of chemicals. Furthermore, methanol could be used as an alternative fuel in the energy distribution infrastructure that exists today, or it could be blended with gasoline.[5] Moreover, methanol can be considered as a "green fuel" if the CO_2 net balance in the atmosphere does not increase when the production of the methanol uses more CO_2 than is produced in the manufacture of H_2.[6]

The main byproducts obtained in the reaction to produce methanol are carbon monoxide and methane, as shown in eqs 3 and 4. One of the current scientific targets is to obtain a catalyst that provides a high conversion and selectivity toward methanol.[7]

$$CO_2 + H_2 \leftrightarrows CO + H_2O \qquad \Delta H_{25\,^\circ C} = 41\ \text{kJ/mol} \quad (3)$$

$$CO_2 + 4H_2 \leftrightarrows CH_4 + 2H_2O \qquad \Delta H_{25\,^\circ C} = -165\ \text{kJ/mol} \quad (4)$$

However, most of the methanol synthesized at present is produced at high pressure and syngas is employed as the reactant. The real goal of this work is the use of carbon dioxide and the transformation of this pollutant into methanol at atmospheric pressure. Several studies[8−12] have been carried out

Received: January 13, 2016
Revised: March 11, 2016
Accepted: March 11, 2016
Published: March 11, 2016

DOI: 10.1021/acs.iecr.6b00170
Ind. Eng. Chem. Res. 2016, 55, 3556−3567

on the hydrogenation of CO_2 to give methanol at atmospheric pressure. The two most widely used active metals, because of their well-known properties and their high efficacy in this reaction, are copper and palladium. In both cases, one of the most commonly used supports used is ZnO. In the case of palladium, the support interacts with the metal to form PdZn alloys and this behavior has been widely studied in the steam reforming of methanol to hydrogen.[13−18]

In the work described here, we combine the advantages offered by PdZn alloys, in terms of the selectivity and activity in the formation of methanol from the hydrogenation of CO_2 and the advantageous characteristics of nanofibers, which are used as the support. Carbon nanofibers (CNFs) are based on ordered parallel graphene layers that are arranged in a specific conformation. These materials have special properties (high mechanical strength, high surface area, low internal mass-transfer resistance, and surface defects for holding catalyst particles) that make them useful in numerous applications, including heterogeneous catalysis, where carbon materials generally have been widely applied.[19,20]

Many papers have been published on the use of carbon materials, carbon nanotubes (CNTs),[21−26] and nanofibers[27] in the hydrogenation of CO_2 to methanol, but all of these references described the use of high pressures and other active metals.

Two types of nanofibers were used in the study reported here, namely fishbone and platelet, which were synthesized at 600 and 450 °C, respectively. It has been reported[28] that the synthesis temperature has an influence of the properties of CNFs. The nanofibers used in this work were reported previously in other papers for the Fischer−Tropsch synthesis[29,30] and the methanation of CO and CO_2.[31]

In the study described here, the influence of the support on the PdZn alloy formed was studied and compared with a reference Pd/ZnO catalyst. Moreover, catalysts with different Pd/Zn molar ratios were used for the hydrogenation of CO_2 to methanol.

This work is the first step in a project that is focused on the synthesis of methanol with a feed of CO_2 and H_2O at atmospheric pressure and using a co-ionic electrochemical membrane reactor. In this step, a catalyst that has a high activity and selectivity toward methanol at higher temperatures is desired. Higher temperatures lead to better ionic conductivity, which, in turn, favors the electrochemical reactor performance. Nanofibers play a fundamental role in this work, because of their excellent conductive properties.

2. EXPERIMENTAL SECTION

2.1. Support/Catalyst Preparation. Different catalysts were used in the different sections of this work. The main catalysts were prepared using carbon nanofibers as support. CNFs with different crystalline structures were prepared by the catalytic decomposition of ethylene over a Ni/SiO_2 catalyst, at 600 °C in the case of fishbone-type nanofiber and at 450 °C for platelet-type nanofiber, according to a literature procedure.[28] The carbon nanofibers were subsequently dissolved in hydrofluoric acid (HF, 70%) for 15 h with vigorous stirring, in order to remove any particles of the Ni/SiO_2 catalyst and recover the carbon material. After this treatment, the nanofibers were filtered off, washed, and dried at 110 °C for 12 h.

Hydrogenation catalysts were prepared by the wet impregnation method. First, the support was placed in a glass vessel and kept under vacuum at room temperature for 2 h to remove water and other impurities adsorbed on the structure. Second, a solution of palladium(II) nitrate ($Pd(NO_3)_2{\cdot}xH_2O$, Aldrich) and zinc nitrate hexahydrate ($Zn(NO_3)_2{\cdot}6H_2O$, Panreac) was poured over the sample, with the appropriate quantities to obtain catalysts with a Pd load of 10 wt % and different Pd/Zn molar ratios. Third, the solvent was removed under vacuum at 90 °C for 2 h. After impregnation, the catalysts were dried at 120 °C overnight.

The calcination was carried out inside the reactor at 500 °C under a N_2 atmosphere to prevent gasification of the CNFs. Prior to the reaction, catalysts were reduced *in situ* in a hydrogen stream (10 vol %) diluted with nitrogen at a flow rate of 25 $cm^3\ min^{-1}$ at 500 °C with a heating rate of 1.3 °C min^{-1}.

Five catalysts were prepared using nanofibers as support. Three additional catalysts were prepared using the same methodology, in order to compare them with those supported on nanofibers: (i) palladium on zinc oxide [ZnO, Panreac] as support; (ii) copper(II) nitrate 3-hydrate [$Cu(NO_3)_2{\cdot}3H_2O$, Panreac] on fishbone nanofibers; and (iii) palladium and zinc on aluminum oxide [Al_2O_3, Alfa Aesar].

The catalysts were denoted as XY/Z, where X indicates the metal(s) used as the active phase, Y the Pd/Zn molar ratio where appropriate, and Z the support used (abbreviated as Fish (fishbone), Plat (platelet), ZnO (zinc oxide), and Al_2O_3 (aluminum oxide)).

2.2. Support/Catalyst Characterization. Palladium and zinc metal loadings were determined by atomic absorption (AA) spectrophotometry on a Spectra Model 220FS analyzer. Samples (ca. 0.5 g) were treated with 2 mL of HCl, 3 mL of HF, and 2 mL of H_2O_2, followed by microwave digestion (250 °C). Surface area/porosity measurements were carried out using a Quadrasorb Model 3SI sorptometer apparatus with N_2 as the sorbate at −196 °C. The samples were outgassed at 250 °C under vacuum (5×10^{-3} Torr) for 12 h prior to analysis. Specific surface areas were determined by the multipoint BET method. Specific total pore volume was evaluated from N_2 uptake at a relative pressure of $P/P_0 = 0.99$. Temperature-programmed reduction (TPR) experiments were conducted in a commercial Micromeritics AutoChem 2950 HP unit with TCD detection. Samples (ca. 0.15 g) were loaded into a U-shaped tube and ramped from room temperature to 900 °C (10 °C min^{-1}), using a reducing gas mixture of 17.5 vol % H_2/Ar (60 $cm^3\ min^{-1}$). Temperature-programmed decomposition (He TPD, H_2 TPD, and CO_2 TPD) analyses were conducted in the same unit. He TPD analysis was carried out using the same procedure as that explained for the TPR, but with the gas changed to helium (99.999% purity, 60 $cm^3\ min^{-1}$). In the case of H_2 TPD, prior to the analysis, the sample was prereduced *in situ* by a gas mixture of 17.5 vol % H_2/Ar (30 $cm^3\ min^{-1}$) at 500 °C with a heating rate of 2.8 °C min^{-1}, and then flushed by an argon stream (99.999% purity, 30 $cm^3\ min^{-1}$) at 500 °C for 30 min to clean the surface, followed by cooling to 160 °C, switching to a H_2 (99.999% purity) stream for hydrogen adsorption at 160 °C for 30 min and subsequently at room temperature for 480 min, and then flushing with the argon stream at room temperature until a stable baseline was observed. The TPD measurement was then conducted from room temperature to 900 °C with a heating rate of 10 °C min^{-1}. CO_2 TPD was conducted as explained for the H_2 TPD; however, after cleaning the surface, it is followed by cooling to 50 °C, switching to a CO_2 (99.999% purity) stream for carbon dioxide adsorption at 50 °C for 30 min, and then flushing with the argon stream at room temperature until a stable baseline

DOI: 10.1021/acs.iecr.6b00170
Ind. Eng. Chem. Res. 2016, 55, 3556−3567

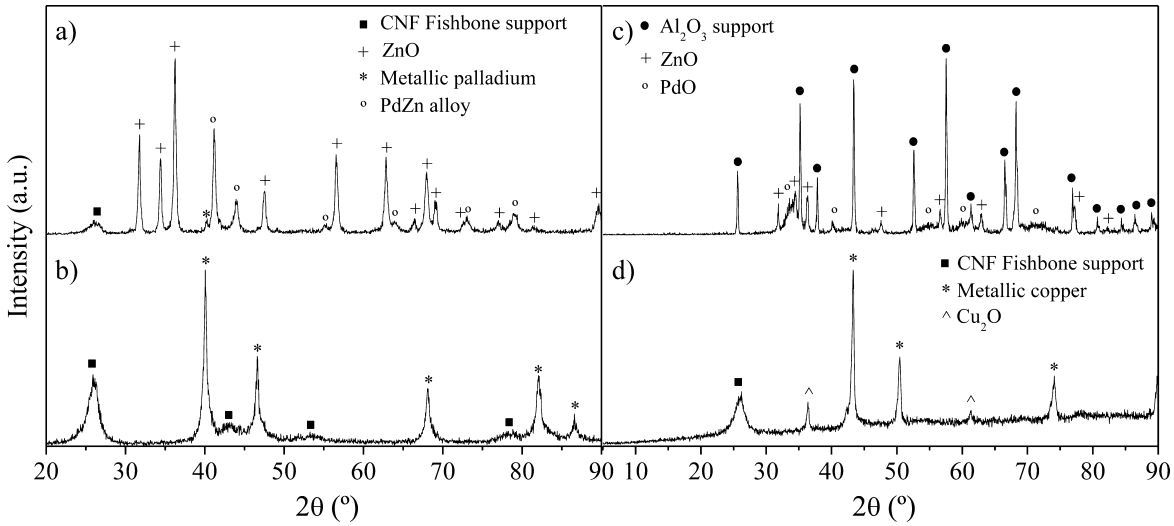

Figure 1. XRD profiles before the reduction step of (a) PdZn0.13/Fish, (b) Pd/Fish, (c) Pd/Al_2O_3, and (d) Cu/Fish.

was observed. The TPD measurement was then conducted from room temperature to 900 °C with a heating rate of 10 °C min^{-1}. The crystallinity of CNFs, the mean crystal size, and the Pd and Zn species were determined by X-ray diffraction (XRD) analyses. The XRD experiments were conducted with a Philips X'Pert instrument using nickel-filtered Cu Kα radiation. Samples were scanned at a rate of 0.02° $step^{-1}$ over a range of $5° \leq 2\theta \leq 90°$ (scan time = 2 s $step^{-1}$). To complete these measurements, transmission electron microscopy (TEM) analyses were carried out on a JEOL Model JEM-4000EX unit with an accelerating voltage of 400 kV. Samples were prepared by ultrasonic dispersion in acetone with a drop of the resulting suspension evaporated onto a holey carbon-supported grid. The external morphology of the different catalyst was evaluated using a Phenom Pro X scanning electron microscopy (SEM) system. This instrument was equipped with an energy-dispersive X-ray spectroscopy (EDX) analyzer to determine the average composition of the samples. Raman spectra of the catalysts were recorded in a SENTERRA Raman spectrometer with 600 lines per mm grating and a laser wavelength of 532 nm at a very low laser power level (<1 mW) to avoid any heating effect.

2.3. Catalyst Activity Measurement. Catalytic performance tests were carried out in a tubular quartz reactor (45 cm length and 1 cm diameter). The catalyst (0.8 g), which had a particle size in the range of 250−500 μm and was not diluted, was placed on a fritted quartz plate located at the end of the reactor. The temperature of the catalyst was measured with a Type K thermocouple (Thermocoax) placed inside the inner quartz tube. The entire reactor was placed in a furnace (Lenton) equipped with a temperature-programmed system. Reaction gases were Praxair certified standards of CO_2 (99.999% purity), H_2 (99.999% purity), and N_2 (99.999% purity). The gas flows were controlled by a set of calibrated mass flowmeters (Brooks, Models 5850 E and 5850 S).

The hydrogenation of CO_2 was carried out at atmospheric pressure in the temperature range of 150−300 °C. The total flow rate, which was a CO_2/H_2 mixture (CO_2/H_2 = 1/9), was maintained at 100 cm^3 min^{-1}. Gas effluents were monitored with a micro gas chromatograph (Varian CP-4900), which contained a PoraPLOT Q column and a molecular sieve column, each of which was connected to a thermal conductivity detection (TCD) system.

3. RESULTS AND DISCUSSION

3.1. Influence of the Carbon Nanofiber (CNF) Support on the PdZn Alloys. The XRD patterns for the samples PdZn0.13/Fish and Pd/Fish before the reduction step are shown in Figures 1a and 1b, respectively. These samples were selected as references, but it should be noted that the same behavior was found for all of the PdZn/nanofiber catalysts. After the calcination step, the main diffraction peaks that one would expect to find should correspond to ZnO and PdO. However, these peaks were not observed at all. The main peaks found correspond to (a) metallic palladium (Joint Committee on Powder Diffraction Standards (JCPDS) File No. 87-0645) for Pd/Fish, and (b) PdZn alloy with a Pd/Zn ratio of 1:1 (JCPDS File No. 06-0620) for PdZn0.13/Fish. In an effort to understand this result, the catalysts and the support were characterized in greater depth.

CNFs are well-known to have oxygen functional groups on their surface.[32−34] Despite the fact that the support was not previously chemically activated with an activating agent (typically alkaline/earth-alkaline hydroxides, as well as different acids or chlorides) to incorporate oxygen groups on its surface, a He TPD from room temperature to 900 °C was performed to investigate the nature of the possible surface groups (Figure 2). The peaks found at the maximum temperature in the range of 70−627 °C correspond to the decomposition of (mainly) carboxylic and lactonic groups to CO_2, and the peak at 700−900 °C is attributed in the literature to decomposition, mainly to CO, of phenolic, carbonyl, anhydride, ether, and quinone groups.[34] Since a reducing agent (CO) is not likely to be formed at the calcination temperature of 500 °C, and according to recent studies,[35,36] it is believed that carbon itself can act as a reducing agent.

In an effort to confirm this theory, two further catalysts were prepared to investigate why the metal was reduced during the calcination step. A $PdZn0.13/Al_2O_3$ catalyst was prepared in an effort to ascertain whether the PdZn alloy is formed on the support during the calcination process. The XRD pattern of this sample (Figure 1c) showed that the PdZn alloy had not been formed. A Cu/Fish catalyst was also prepared in order to

DOI: 10.1021/acs.iecr.6b00170
Ind. Eng. Chem. Res. 2016, 55, 3556−3567

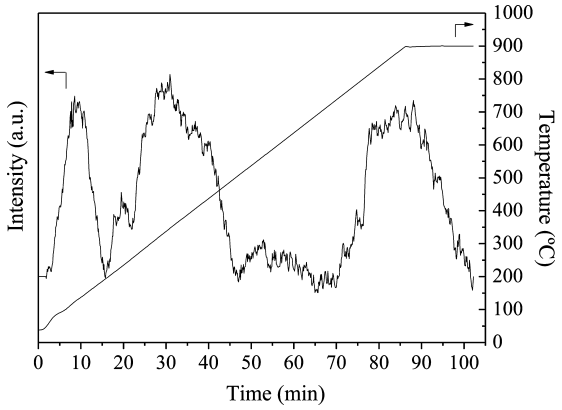

Figure 2. Temperature-programmed reduction in helium (He TPD) of the fishbone carbon nanofiber (CNF) support.

determine whether the same behavior occurs with other metals (Figure 1d). The main peaks correspond to metallic copper (JCPDS File No. 85-1326), which indicates that copper had indeed been reduced. This result suggests that the carbon nanofibers are the only species responsible for the formation of PdZn and metallic palladium.

Since the PdZn alloy is formed without a reduction step, and the PdZn alloy is the active phase for the production of methanol, the PdZn0.13/Fish prior to reduction was used as a reference to determine whether the reduction step is necessary in the process. The characterization of this catalyst will be described in the next section, along with the corresponding catalytic results for the hydrogenation of carbon dioxide.

3.2. Influence of the Pd/Zn Molar Ratio. Four catalysts were prepared in order to study the influence that the Pd/Zn molar ratio has on the hydrogenation of carbon dioxide. The XRD results for the different catalysts are shown in Figure 3, including those for the Pd/Fish used as a reference, to confirm the PdZn alloy behavior for methanol production. The decrease in the Pd/Zn molar ratio means that the main peaks are due to PdZn alloy in the case of PdZn0.75/Fish (Figure 3c) and ZnO in the case of PdZn0.13/Fish (Figure 3a). Furthermore, the

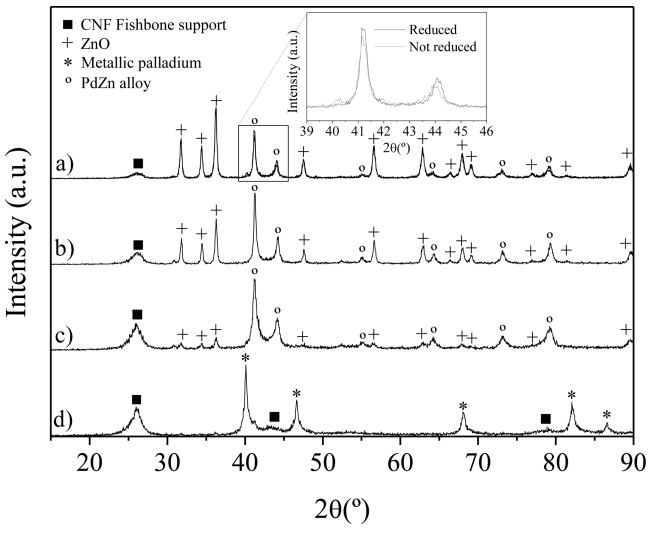

Figure 3. XRD profiles of (a) PdZn0.13/Fish before and after reduction, (b) PdZn0.25/Fish, (c) PdZn0.75/Fish, and (d) Pd/Fish after reduction.

diffractograms of the PdZn0.13/Fish sample before and after reduction overlap each other and they appear to be very similar, in relative terms. It can be seen from the enlargement that the intensities of the main peaks for the PdZn alloy (JCPDS File No. 06-620) are higher in the case of the reduced catalyst. A higher intensity in the XRD peaks is due to a larger amount of PdZn alloy in the catalyst and this, in turn, leads to a higher methanol production.[8] This situation is consistent with the catalytic results (Figure 4), which show that the reduced catalyst has higher activity and selectivity toward methanol. Therefore, the nonreduced PdZn0.13/Fish was discarded. A reduction step is still necessary in order to obtain higher methanol formation rates. It is in agreement with the different changes in the Pd/ZnO crystal structure during the reduction process,[15] where it is modified in different steps as follows: PdO/ZnO → Pd/ZnO → PdZnO1−x/ZnO → amorphous PdZn alloy/ZnO → crystalline PdZn alloy/ZnO. Hence, the nonreduced PdZn0.13/Fish sample would not have completed all these steps during the autoreduction and, consequently, it is still necessary an additional reduction under H_2 atmosphere. Moreover, Pd/Fish gave rise to the lowest methanol formation rate and the highest methane formation rate, because metallic palladium (JCPDS File No. 87-0645) leads to the formation of carbon monoxide and methane.[37] The Pd/Zn molar ratio also modifies the catalytic performance. The methanol formation rate curve is displaced to higher temperatures when the Pd/Zn molar ratio is decreased, but the maximum of this curve does not change. The formation of byproducts (CO and CH_4) is favored by a higher Pd/Zn molar ratio and, as a consequence, the selectivity to methanol is decreased.

The results in Table 1 show that a lower Pd/Zn molar ratio leads to a higher PdZn alloy particle size and to a lower surface area, total pore volume, and average pore radius in the support. The presence of larger species on the same surface can lead to blockage of the pores and this would lower the free surface area. Higher Pd/Zn molar ratios lead to smaller particles, which are more active and lead to higher CO_2 conversion and lower selectivity toward methanol at higher temperatures. This situation is consistent with the TEM analysis carried out on the catalysts PdZn0.13/Fish (Figure 5a) and PdZn0.75/Fish (Figure 5b). It can be appreciated that, in the former case, the PdZn alloy is supported on carbon nanofibers and zinc oxide. As a consequence, the real support is a combination of these two compounds. For the PdZn0.75/Fish sample (Figure 5b), all of the images indicate that the alloy is supported on nanofibers. The particle size distribution is represented in Figure 5d, where more than 500 particles were measured. Both of the catalysts show a Gaussian particle distribution. The particle distribution shows that the PdZn0.75/Fish sample has a much higher proportion of smaller particles. Smaller particles imply a higher number of active sites and, consequently, a higher conversion, which, at the same time, involves a lower selectivity at higher temperatures. Interestingly, the maximum methanol formation rate is approximately the same for the three PdZn/Fish samples. It suggests that, from a certain number of PdZn alloy particles, the maximum methanol production is reached, regardless of further changes on the Pd/Zn molar ratio.

CO_2 TPD (Figure 6a) and H_2 TPD (Figure 6b) were carried out in order to study the adsorption behavior of these reactants on the catalysts. The desorption quantities are listed in Table 2. In both cases, the catalyst exhibited two desorption peaks. The first peak, at ∼50 °C, is attributed to the loss of weakly

DOI: 10.1021/acs.iecr.6b00170
Ind. Eng. Chem. Res. 2016, 55, 3556−3567

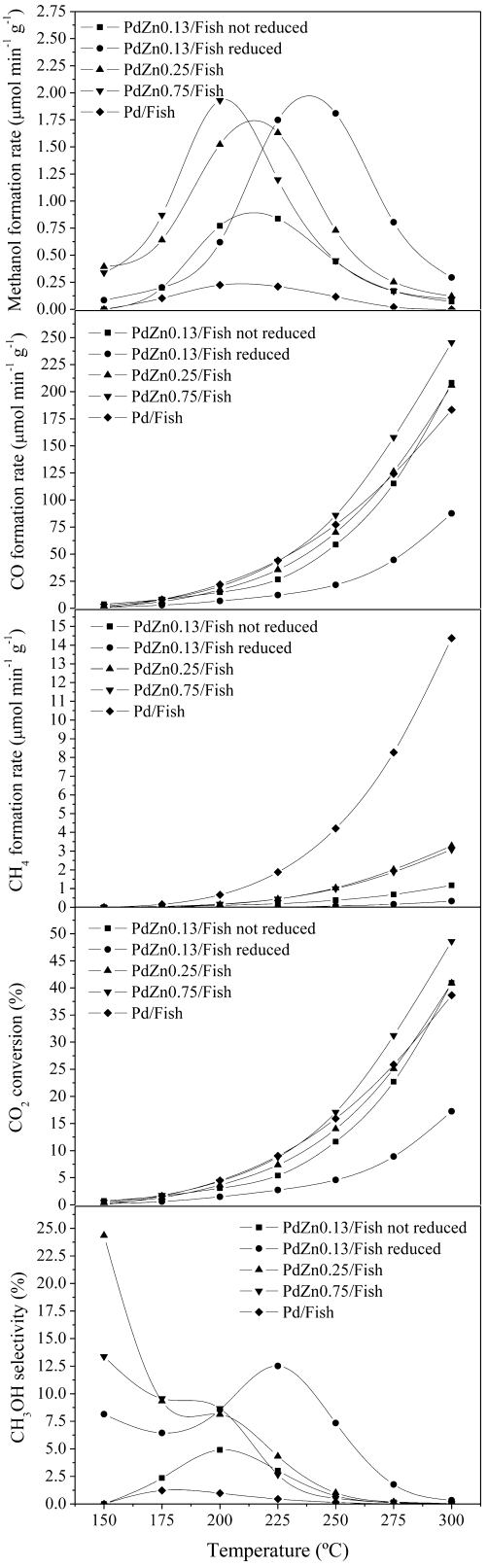

Figure 4. Catalytic activity for the catalysts with different Pd/Zn molar ratios. Reaction conditions: CO_2/H_2 = 1/9 and W/F = 0.008 g min cm^{-3}.

adsorbed CO_2 and H_2; the second peak, which is observed in the temperature range of 500−900 °C, is probably due to a combination of different peaks. It has been reported in the literature that the strength of the CO_2 binding is related to the calcination temperature.[27] In this work, however, the strength of the CO_2 and H_2 binding is related to the Pd/Zn molar ratio. Although this adsorption does not have any influence on the maximum methanol formation rate, there is a link between CO_2 and H_2 adsorption and the temperature at which the highest formation rate toward methanol was obtained. This situation can clearly be seen in Figure 6c, in which an exponential link between reactant adsorption and the temperature with the highest methanol formation rate can be observed. This behavior is probably due to the equilibrium (eq 2). If the maximum methanol formation rate is the same but the concentration of the reactants on the surface of the catalyst increases due to the effect of better adsorption, then that maximum should be obtained at a higher temperature. An in-depth study using kinetic expressions would be necessary to confirm this point, but an approximate link has been demonstrated.

TPR profiles are shown in Figure 7. The TPR of the sample Pd/Fish was carried out in order to determine the differences that exist when Zn is absent from the catalyst. The high inverse peak found at ∼50 °C is assigned to PdH_x decomposition to give metallic palladium. According to literature data,[16,18] PdH_x is formed rapidly when hydrogen is fed over the catalyst at room temperature, with PdO converted to PdH_x. In the profiles obtained in this work, this H_2 consumption peak is not observed, because the hydrogen is in contact with the catalyst at room temperature before the TPR experiment starts. For the other catalysts, the inverse peak was observed to a lesser extent, which indicates that the metallic palladium is present in all of the catalysts but at lower levels. The large peak at ∼600 °C is associated with an onset of low-temperature gasification of the support, which is catalyzed in the presence of metallic palladium.[38] For the catalysts with Zn, the broad H_2 consumption found in the range of 400−600 °C can be attributed to the different changes that occur during the formation of the PdZn alloys,[15,37] and the peaks at higher temperatures can be assigned to the gasification of nanofibers and the different degrees of carbon surface oxidation.[39]

The Pd/Zn molar ratio that was selected as being the most appropriate for the hydrogenation of carbon dioxide in this work was 0.13. The PdZn0.13/Fish catalyst is able to work at higher temperatures with higher selectivity toward methanol. As explained in the Introduction, one future objective of the project is the deposition of the catalyst onto the cathode of an electrochemical reactor, in which ions would move more easily at high temperatures. As a consequence, PdZn0.13/Fish was selected for the next stage of the study.

3.3. Influence of the Different Nanofiber Supports.

Two types of nanofibers were compared in this work: fishbone and platelet. The only difference between these materials was the synthesis temperature: 600 °C for fishbone and 450 °C for platelet. A Pd/ZnO catalyst was also prepared as a reference sample in order to compare it with the nanofiber-based catalysts. The reference catalyst was prepared using the best preparation conditions identified in a previous study.[37]

The XRD patterns of the platelet nanofiber-based catalysts before reduction (not shown here) showed the same trend as found for the fishbone nanofibers, where the carbon itself acted as a reducing agent.

The XRD patterns after reduction for the nanofiber-based catalysts are shown in Figure 8. The patterns are fairly similar but it can be seen from the enlargement that the intensities of the main peaks for the PdZn alloy (JCPDS File No. 87-0645) are higher for the PdZn0.13/Fish catalyst. This finding suggests

DOI: 10.1021/acs.iecr.6b00170
Ind. Eng. Chem. Res. 2016, 55, 3556−3567

Table 1. Main Physical Properties of the Fishbone Catalysts

	fishbone support	PdZn0.13/Fish not reduced	PdZn0.13/Fish	PdZn0.25/Fish	PdZn0.75/Fish	Pd/Fish
Pd loading (wt %)		12.98	12.98	12.25	11.25	15.4
Zn loading (wt %)		45.72	45.72	30.22	9.68	
surface area[a] ($m^2\ g^{-1}$)	116.58	56.66	53.39	82.77	103.0	97.9
total pore volume[b] ($\times 10^2\ cm^3\ g^{-1}$)	61.45	24.05	20.15	40.58	52.0	34.9
average pore radius[b] (Å)	105.4	84.88	75.48	98.04	100.9	71.4
particle diameter PdZn from XRD before reaction (nm)			56.1	54.3	26.8	43.6
particle diameter PdZn from XRD after reaction (nm)			62.3	55.9	31.4	45.2

[a]Measurement error ≈ 5 m^2/g. [b]Measurement error of <5%.

a higher level of crystalline PdZn alloy in this sample, which could be due to the influence that the support has on the PdZn alloy formation. This influence is also shown by the slight displacement to higher angles 2θ (deg) of the PdZn alloy peaks for the PdZn0.13/Plat sample. It means that contraction between lattices of the PdZn alloy occurs. It indicates that a change in the lattice parameters of the PdZn alloy tetragonal system (JCPDS File No. 87-0645) has occurred. These lattice parameters were calculated based on Bragg's law (eq 5) and the formula for the tetragonal system crystal structure (eq 6):

$$n\lambda = 2d \sin\theta \tag{5}$$

$$d = \frac{a}{\sqrt{h^2 + k^2 + l^2\left(\frac{a^2}{c^2}\right)}} \tag{6}$$

The lattice parameters changed from a = 0.410 nm and c = 0.335, for the PdZn0.13/Fish catalyst, to a = 0.409 and c = 0.333, for the PdZn0.13/Plat sample. According to Kazuki et al.,[40] this contraction between lattices is related to a slight decrease in the Pd/Zn ratio of the alloy. Therefore, the alloy formed in the PdZn0.13/Plat catalyst has a higher amount of zinc in its structure. Preliminary calculations of the percentage of zinc incorporated to the structure were made using Vergard's law, which has been used for other solid mixtures, such as Pt-metal alloys.[41,42] Note that, taking into account the limitations of this law,[43] this number is just a rough approximation. According to these calculations, the new PdZn alloy formed in the PdZn0.13/Plat catalyst would be $Pd_{48.5}Zn_{51.5}$.

The main physical properties of the catalysts are provided in Table 3. A lower PdZn alloy particle size was found for the platelet-based catalysts, probably because of the higher surface area of this support. It could be expected that this sample would provide higher conversions. However, the catalytic results (Figure 9 and Table 4) did not show a clear relationship between the PdZn alloy particle size and the catalyst performance. It seems clear that the different supports play an important role in the interaction with the PdZn alloy, considered as the active phase in the production of methanol. The CO_2 conversion, methanol selectivity, and methanol yield are shown in Table 4. The highlighted values show that the Pd/ZnO catalyst works better at lower temperatures, while the PdZn0.13/Plat catalyst works better at higher temperatures. Additional characterization was carried out in an effort to understand the differences between the different supports.

As mentioned above, the difference between fishbone and platelet nanofibers is the synthesis temperature. It is well-known that an increase in the reaction temperature leads to more crystalline structures.[44] The graphitic character of the supports can be evaluated by XRD. The data for the interlayer spacing (d_{002}), average crystalline parameter (L_C), and average number of planes of graphite crystals (npg), which are listed in Table 3, provide a measure of the structural order of the materials. The order increased with both decreasing values of d_{002} and increasing values of L_C and npg. Therefore, the structural order is fishbone > platelet. A more disordered structural nature means that the materials have a higher surface area (and certainly a higher surface area was found for the more-disordered platelet nanofibers), more defects, exposed edge planes and surface C−H/O−H groups. This structure could play an important role in the PdZn alloy deposition and, consequently, on the catalytic activity. Structural features were further assessed by Raman spectroscopy (see Figure 10). Raman spectra of the nanofibers supports exhibited two peaks, habitually denoted as D- and G-bands, at ca. 1354 and 1600 cm^{-1}, respectively. The D-band has been attributed to the presence of defects and/or curvature in the carbon structure,[45,46] while the G-band is associated with well-ordered structures.[47,48] Thus, the relative intensities of D- and G-bands (I_D/I_G) can be used as an index to assess graphitic character. The following structural order was found: fishbone (I_D/I_G = 1.02) > platelet (I_D/I_G = 1.18). In addition, the differences found in the values of intensity of the D-band mean that platelet and fishbone supports could have different curvatures. It has been reported in the literature[49] that the interaction of the transition metals with the nanofibers is dependent on their curvature. Thus, this observation is more proof that the interaction with the PdZn alloy is different for both supports.

TEM images at a resolution of 100 nm seem to show, at first glance, that the PdZn0.13/Plat (Figure 5c) and PdZn0.13/Fish (Figure 5a) catalysts are quite similar. However, the structures of these two materials are quite different, as shown in Figures 5f and 5g. The platelet structure has hexagonal planes perpendicular to the fiber axis, and the graphene layers of the fishbone structure terminate on the surface with a defined inclination angle. Some previous papers have shown that this orientation of graphene sheets can significantly influence the catalytic behavior and the selectivity toward different compounds.[50−53] The metal particle distribution (Figure 5e) shows some characteristics that are consistent with the PdZn alloy particle size obtained by XRD. The Gaussian distribution of these particles is shifted to lower particle sizes in the order PdZn0.13/Plat < PdZn0.13/Fish ≅ Pd/ZnO. SEM images for the PdZn0.13/Fish catalyst (Figure 5h) and for the PdZn0.13/Plat sample (Figure 5i) show that the external morphology of both catalysts is quite different. EDX analysis confirmed that the PdZn0.13/Fish catalyst showed a higher percentage of palladium. It could be due to the position of the PdZn alloy particles. These particles could be hidden in the pores of the

DOI: 10.1021/acs.iecr.6b00170
Ind. Eng. Chem. Res. 2016, 55, 3556−3567

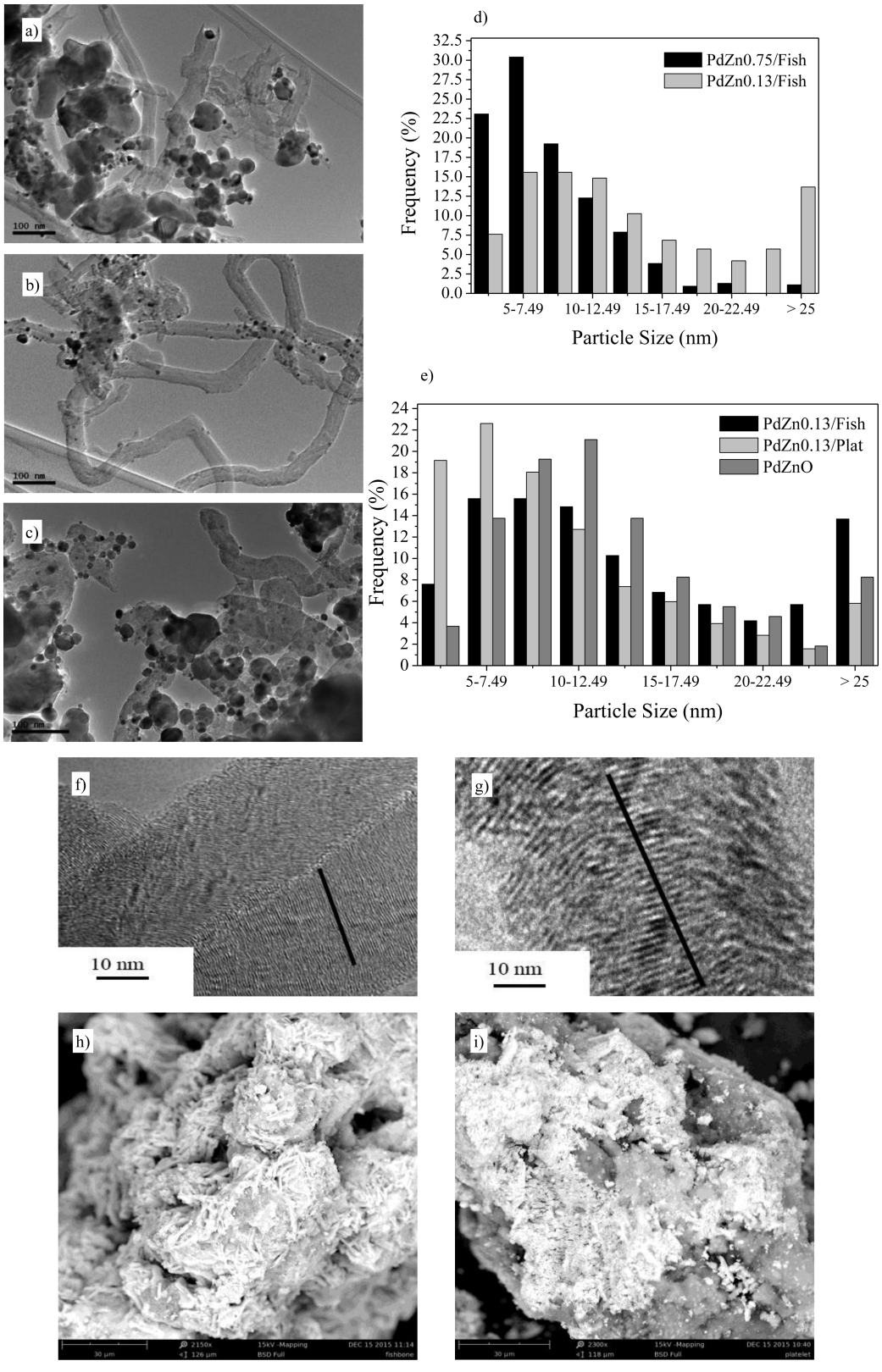

Figure 5. High-resolution TEM images of (a) PdZn0.13/Fish, (b) PdZn0.75/Fish, and (c) PdZn0.13/Plat. Metal particle distribution of (d) PdZn0.75/Fish and PdZn0.13/Fish and (e) PdZn0.13/Fish, PdZn0.13/Plat, and Pd/ZnO. High-resolution TEM images of (f) fishbone support and (g) platelet support. SEM images of (h) PdZn0.13/Fish and (i) PdZn0.13/Plat.

structure of the PdZn0.13/Plat catalyst, but are located on the surface for the PdZn0.13/Fish catalyst. Such a phenomenon would have an effect on the catalytic behavior, with the PdZn0.13/Fish sample being more active for the CO_2 hydrogenation and, therefore, less selective toward methanol, because of the greater level of PdZn alloy particles exposed.

The CO_2 and H_2 TPD profiles are shown in Figure 11. The same exponential relationship found in the previous section,

DOI: 10.1021/acs.iecr.6b00170
Ind. Eng. Chem. Res. 2016, 55, 3556−3567

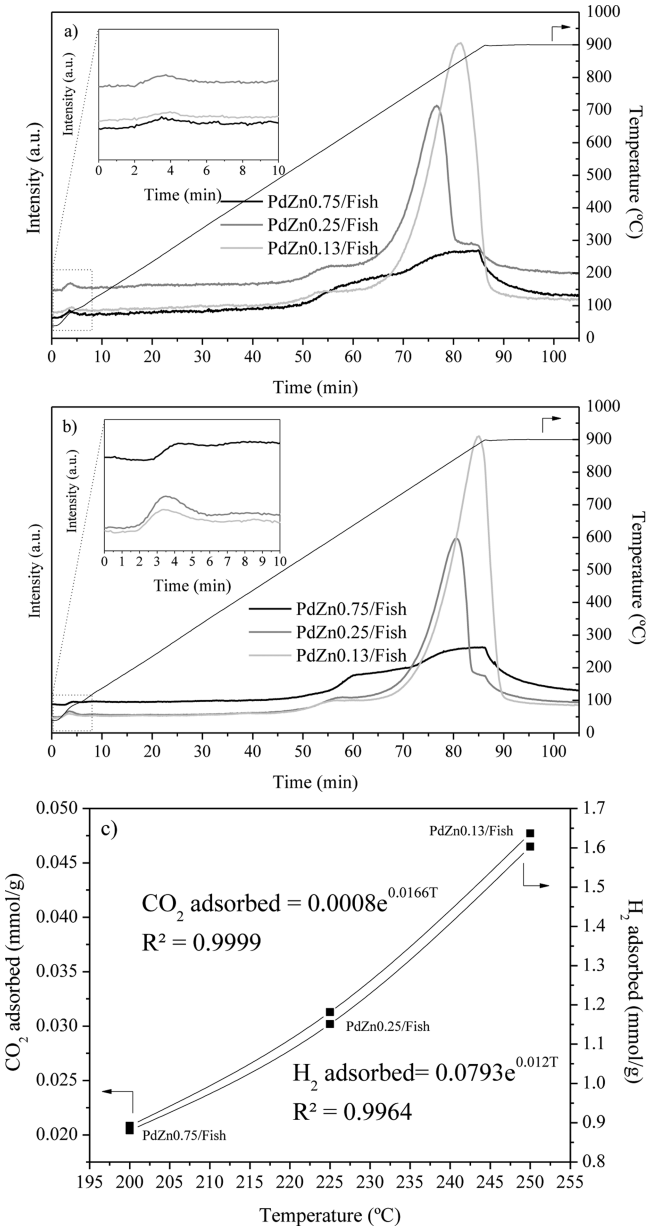

Figure 6. (a) CO_2 TPD, (b) H_2 TPD, and (c) exponential relationship between the reactants adsorbed and the temperature at which the highest methanol formation rate was obtained for the catalysts with different Pd/Zn molar ratios.

Table 2. Total Amounts of H_2 and CO_2 Released in CO_2 and H_2 Temperature-Programmed Desorptions (TPDs)

catalyst	CO_2 (mmol/g)	H_2 (mmol/g)
PdZn0.13/Fish	0.047 ± 0.003	1.603 ± 0.034
PdZn0.25/Fish	0.031 ± 0.002	1.151 ± 0.027
PdZn0.75/Fish	0.021 ± 0.002	0.880 ± 0.025

but with an additional point, was again observed, which confirmed the correlation between the amount of reactant adsorbed and the temperature with the highest methanol production. The nanofiber TPD profiles showed the same peaks as in the previous study. The PdZn0.13/Plat catalyst gave the highest values for CO_2 and H_2 adsorptions. This result is understandable, bearing in mind the previous discussion on the catalyst structure. It is interesting to note that the Pd/ZnO

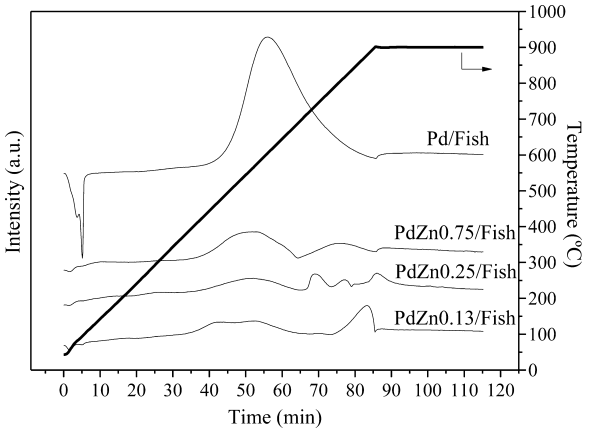

Figure 7. Temperature-programmed reduction (TPR) profiles. Comparison between the catalysts with different Pd/Zn molar ratios.

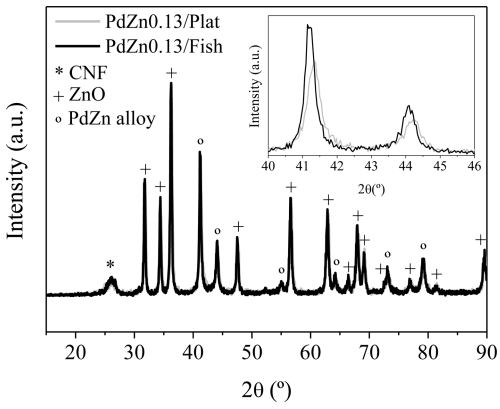

Figure 8. XRD profiles after the reduction step of PdZn0.13/Fish and PdZn0.13/Plat.

Table 3. Main Physical Properties of the Catalysts with Different Supports

Main Physical Properties			
	PdZn0.13/Fish	PdZn0.13/Plat	PdZnO
Pd loading (wt %)	12.98	10.92	10.90
Zn loading (wt %)	45.72	40.20	
surface area[a] (m^2 g^{-1})	53.39	72.20	8.60
total pore volume[b] ($\times 10^2$ cm^3 g^{-1})	20.15	24.91	3.40
average pore radius[b] (Å)	75.48	68.99	79.10
particle diameter PdZn from XRD before reaction (nm)	56.1	38.6	60.8
particle diameter PdZn from XRD after reaction (nm)	62.3	42.3	
average interlayer spacing, d_{002} (nm)	0.3406	0.3437	
number of grapheme planes in the crystallites, npg[c]	29.2	21.6	
average crystal domain size along a direction perpendicular to the basal planes, L_C (nm)	9.95	7.41	
H_2 consumption TPR analysis (μmol/g)	139	741	208
Supports			
	fishbone	platelet	ZnO
surface area[a] (m^2 g^{-1})	116.58	150.94	7.23

[a]Measurement error ≈ 5 m^2/g. [b]Measurement error of <5%. [c]npg = L_C/d_{002}.

DOI: 10.1021/acs.iecr.6b00170
Ind. Eng. Chem. Res. 2016, 55, 3556−3567

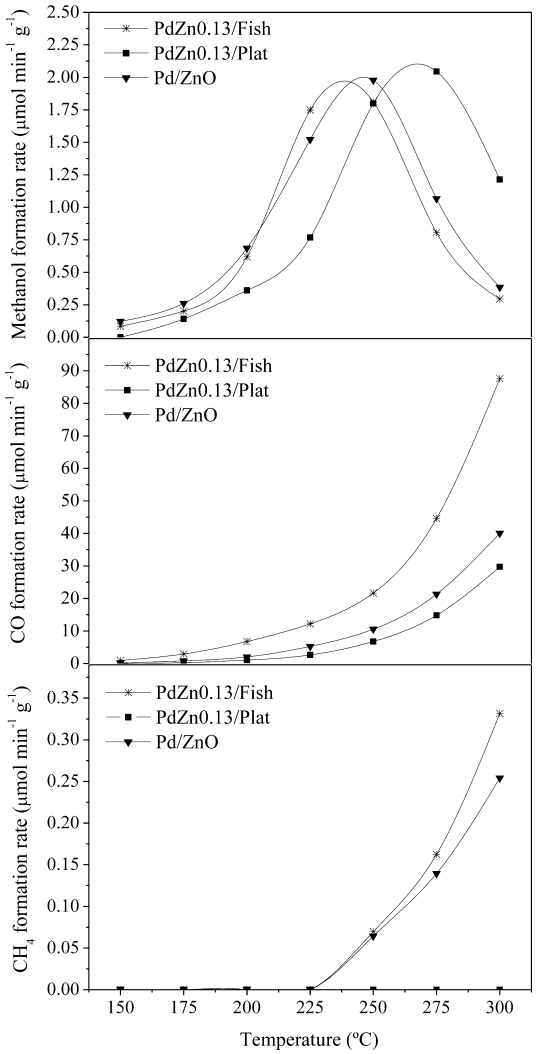

Figure 9. Catalytic activity for the catalysts with different supports. Reaction conditions: CO_2/H_2 = 1/9 and W/F = 0.008 g min cm^{-3}.

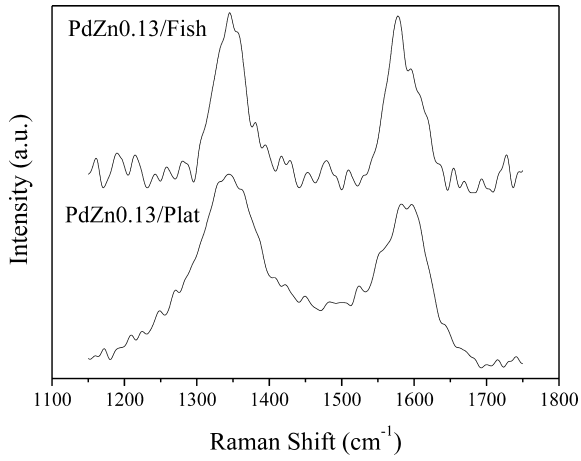

Figure 10. Raman spectra for the PdZn0.13/Fish (I_D/I_G = 1.02) and PdZn0.13/Plat (I_D/I_G = 1.18).

sample did not adsorb any reactant. Therefore, the adsorption of compounds is clearly influenced by the support. In other carbon materials, such as carbon nanotubes (CNTs),[22,25] it has been observed that the H_2 species adsorbed on the catalyst could generate surface microenvironments with high stationary-state concentrations of H-adspecies on the catalyst. These active H-adspecies could be readily transferred to active sites via hydrogen spillover, thus increasing the specific reaction rate of the hydrogenation. In our case, such an increase in the reaction rate was not observed but, as explained previously, it increases the temperature at which the highest methanol rate is obtained (due to the displacement of the equilibrium).

TPR analysis (Figure 12) showed the same peaks that were explained in the previous section. The two peaks observed at ∼300−500 °C for the Pd/ZnO catalyst are shifted to higher temperatures for the nanofiber-based samples. The PdZn0.13/Plat catalyst gave rise to the largest peak located at the highest temperature (∼600 °C). The peak displacement at higher temperatures can be attributed to greater metal−support interaction, which is influenced by the orientation of graphene sheets.[54,55]

On balance, we suggest that the combination of a different structural nature with a different graphene sheets orientation, the different ratio Pd/Zn in the alloy, higher reactant adsorption on the surface and a major metal−support interaction can explain the higher activity and selectivity toward methanol of the PdZn0.13/Plat catalyst.

Finally, in order to check the stability of this catalyst, an additional experiment of 48 h was carried out with the same reaction conditions (CO_2/H_2 = 1/9 and W/F = 0.008 g min cm^{-3}) at the temperature where more methanol was obtained (275 °C). The results (Figure 13) show a high stability for the PdZn0.13/Plat catalyst. The CO_2 conversion was kept constant (relative change of −1.4%), not increasing the undesirable products and obtaining similar values of methanol formation rate (relative change of 2.6%). As a consequence of its properties and stability, this is a promising catalyst to carry out this reaction in an electrochemical reactor.

Table 4. Conversion, Methanol Selectivity, and Methanol Yield Comparison between the Different Supports

	PdZn0.13/Fish			PdZn0.13/Plat			PdZnO		
temperature (°C)	CO_2 conversion, X (%)	CH_3OH selectivity, S (%)	CH_3OH yield (%)	CO_2 conversion, X (%)	CH_3OH selectivity, S (%)	CH_3OH yield (%)	CO_2 conversion, X (%)	CH_3OH selectivity, S (%)	CH_3OH yield (%)
150	0.20	8.14	1.66	0	0	0	0.05	43.23	2.35
175	0.61	6.44	3.95	0.08	33.95	2.77	0.21	27.80	5.75
200	1.51	8.54	12.85	0.28	25.22	7.05	0.52	25.60	13.40
225	2.73	12.52	34.17	0.66	22.63	15.01	1.27	22.81	28.98
250	4.58	7.34	33.63	1.68	20.95	35.16	2.45	15.79	38.67
275	8.90	1.77	15.72	3.29	12.14	39.99	4.40	4.74	20.85
300	17.25	0.33	5.76	6.04	3.93	23.73	7.95	0.98	7.79

DOI: 10.1021/acs.iecr.6b00170
Ind. Eng. Chem. Res. 2016, 55, 3556−3567

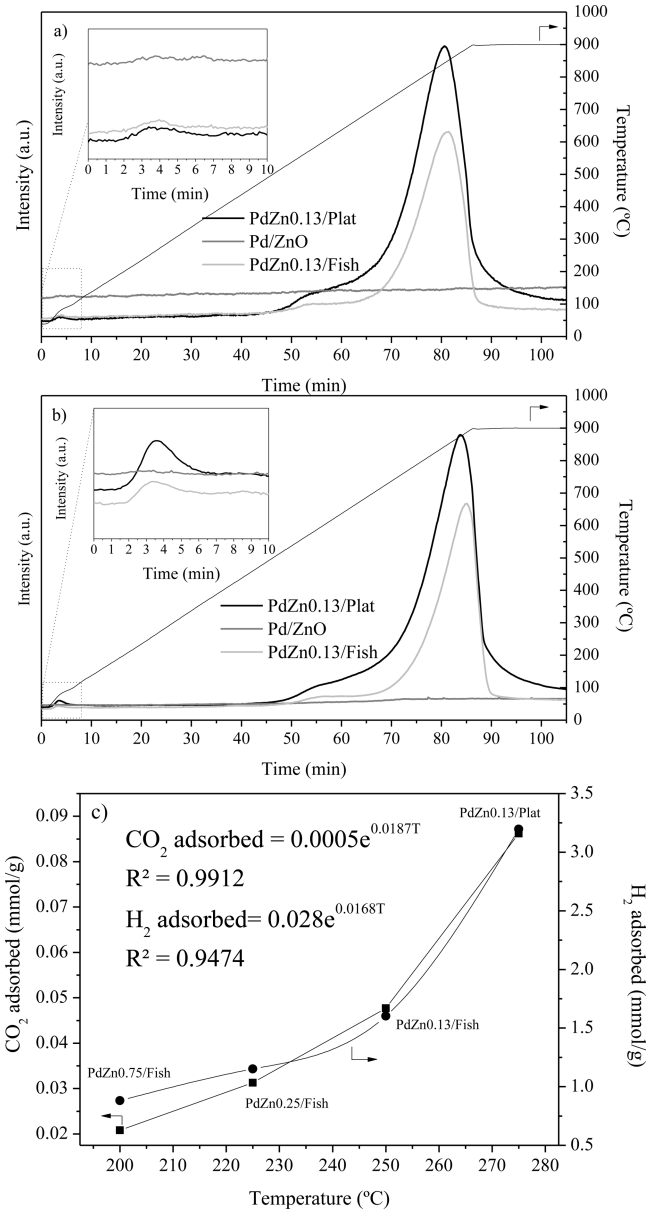

Figure 11. (a) CO_2 TPD and (b) H_2 TPD. (c) Exponential link between the reactants adsorbed and the temperature at which the highest methanol formation rate was obtained for the catalysts with different supports.

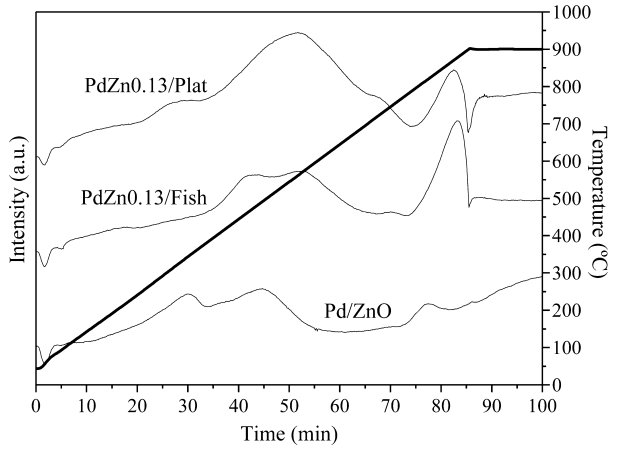

Figure 12. Temperature-programmed reduction (TPR) profiles. Comparison between the catalysts with different supports.

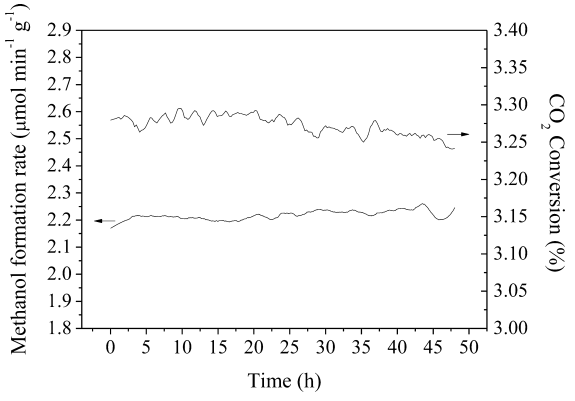

Figure 13. Catalytic stability for the PdZn0.13/Plat catalyst. Reaction conditions: 275 °C, CO_2/H_2 = 1/9 and W/F = 0.008 g min cm^{-3}.

4. CONCLUSIONS

The following conclusions can be drawn from this study:

- The PdZn catalysts supported on fishbone and platelet nanofibers can be autoreduced by the supports in an inert atmosphere of N_2 at 500 °C. However, the catalysts that were reduced after that point showed a better performance.
- A decrease in the Pd/Zn molar ratio leads to displacement of the methanol formation rate curve toward higher temperatures. An increase in the Pd/Zn molar ratio leads to the formation of smaller particles, which are more active and, therefore, less selective to methanol at higher temperatures.
- Based on the equilibrium reaction, an exponential relation was found between the amount of reactant (CO_2 and H_2) adsorbed on the catalyst and the temperature at which the higher methanol formation rate is obtained. This relation was tested for the fishbone nanofiber-based catalysts and was confirmed with the platelet-based samples.
- Based on XRD analysis, an alloy with a different Pd/Zn ratio ($Pd_{48.5}Zn_{51.5}$) was found in the platelet support.
- The higher activity and selectivity toward methanol at higher temperature for the PdZn0.13/Plat catalyst was attributed to different factors: a higher reactant adsorption, a different ratio Pd/Zn in the alloy, and a greater metal−support interaction, because of the different graphene sheet orientations.
- The PdZn0.13/Plat has demonstrated good stability in the production of methanol in a 48 h experiment.
- The platelet nanofiber-based catalyst has properties that are good enough for it to be used as the cathode in an electrochemical reaction for methanol synthesis.

AUTHOR INFORMATION

Corresponding Author

*Tel.: +34 926295300. Fax: +34 926295256. E-mail: Javier.Diez@uclm.es.

Notes

The authors declare no competing financial interest.

ACKNOWLEDGMENTS

The authors would like to thank the Ministerio de Economía y Competitividad (Project No. PCIN-2013-183), the Sociedad Española de Catálisis (SECAT Introducción a la Investigación

DOI: 10.1021/acs.iecr.6b00170
Ind. Eng. Chem. Res. 2016, 55, 3556−3567

en Catálisis grant) and the Spanish government (Grant No. FPU13/00727) for their financial support.

REFERENCES

(1) IEA Statistics. *CO_2 Emissions from Fuel Combustion*, 2014 Edition; International Energy Agency: Paris, 2014.
(2) *World Energy Outlook 2014*; International Energy Agency: Paris, 2014.
(3) Saeidi, S.; Amin, N. A. S.; Rahimpour, M. R. Hydrogenation of CO_2 to value-added products—A review and potential future developments. *J. CO_2 Util.* **2014**, *5*, 66−81.
(4) Raudaskoski, R.; Turpeinen, E.; Lenkkeri, R.; Pongrácz, E.; Keiski, R. L. Catalytic activation of CO_2: Use of a secondary CO_2 for the production of synthesis gas and for methanol synthesis over copper-based zirconia-containing catalysts. *Catal. Today* **2009**, *144*, 318−323.
(5) Olah, G. A. Beyond Oil and Gas: The Methanol Economy. *Angew. Chem., Int. Ed.* **2005**, *44*, 2636−2639.
(6) Jadhav, S. G.; Vaidya, P. D.; Bhanage, B. M.; Joshi, J. B. Catalytic carbon dioxide hydrogenation to methanol: A review of recent studies. *Chem. Eng. Res. Des.* **2014**, *92*, 2557−2567.
(7) Ganesh, I. Conversion of carbon dioxide into methanol—A potential liquid fuel: Fundamental challenges and opportunities (a review). *Renewable Sustainable Energy Rev.* **2014**, *31*, 221−257.
(8) Iwasa, N.; Suzuki, H.; Terashita, M.; Arai, M.; Takezawa, N. Methanol synthesis from CO_2 under atmospheric pressure over supported Pd catalysts. *Catal. Lett.* **2004**, *96*, 75−78.
(9) Fujita, S.i.; Usui, M.; Ohara, E.; Takezawa, N. Methanol synthesis from carbon dioxide at atmospheric pressure over Cu/ZnO catalyst. Role of methoxide species formed on ZnO support. *Catal. Lett.* **1992**, *13*, 349−358.
(10) Fujita, S.; Usui, M.; Hanada, T.; Takezawa, N. Methanol synthesis from CO_2−H_2 and from CO−H_2 under atmospheric pressure over Pd and Cu catalysts. *React. Kinet. Catal. Lett.* **1995**, *56*, 15−19.
(11) Fujita, S. I.; Kanamori, Y.; Satriyo, A. M.; Takezawa, N. Methanol synthesis from CO_2 over Cu/ZnO catalysts prepared from various coprecipitated precursors. *Catal. Today* **1998**, *45*, 241−244.
(12) Maniecki, T. P.; Mierczynski, P.; Maniukiewicz, W.; Bawolak, K.; Gebauer, D.; Jozwiak, W. K. Bimetallic Au-Cu, Ag-Cu/$CrAl_3O_6$ catalysts for methanol synthesis. *Catal. Lett.* **2009**, *130*, 481−488.
(13) Chin, Y. H.; Wang, Y.; Dagle, R. A.; Shari Li, X. S. Methanol steam reforming over Pd/ZnO: Catalyst preparation and pretreatment studies. *Fuel Process. Technol.* **2003**, *83*, 193−201.
(14) Chin, Y. H.; Dagle, R.; Hu, J.; Dohnalkova, A. C.; Wang, Y. Steam reforming of methanol over highly active Pd/ZnO catalyst. *Catal. Today* **2002**, *77*, 79−88.
(15) Wang, Y.; Zhang, J.; Xu, H. Interaction between Pd and ZnO during Reduction of Pd/ZnO Catalyst for Steam Reforming of Methanol to Hydrogen. *Chin. J. Catal.* **2006**, *27*, 217−222.
(16) Iwasa, N.; Mayanagi, T.; Ogawa, N.; Sakata, K.; Takezawa, N. New catalytic functions of Pd-Zn, Pd-Ga, Pd-In, Pt-Zn, Pt-Ga and Pt-in alloys in the conversions of methanol. *Catal. Lett.* **1998**, *54*, 119−123.
(17) Zhang, H.; Sun, J.; Dagle, V. L.; Halevi, B.; Datye, A. K.; Wang, Y. Influence of ZnO facets on Pd/ZnO catalysts for methanol steam reforming. *ACS Catal.* **2014**, *4*, 2379−2386.
(18) Iwasa, N.; Masuda, S.; Ogawa, N.; Takezawa, N. Steam reforming of methanol over Pd/ZnO: Effect of the formation of PdZn alloys upon the reaction. *Appl. Catal., A* **1995**, *125*, 145−157.
(19) Su, D. S.; Perathoner, S.; Centi, G. Nanocarbons for the Development of Advanced Catalysts. *Chem. Rev.* **2013**, *113*, 5782−5816.
(20) Xiong, H.; Jewell, L. L.; Coville, N. J. Shaped Carbons as Supports for the Catalytic Conversion of Syngas to Clean Fuels. *ACS Catal.* **2015**, *5*, 2640−2658.
(21) Liang, X. L.; Xie, J. R.; Liu, Z. M. A Novel Pd-decorated Carbon Nanotubes-Promoted Pd-ZnO Catalyst for CO_2 Hydrogenation to Methanol. *Catal. Lett.* **2015**, *145*, 1138−1147.
(22) Liang, X. L.; Dong, X.; Lin, G. D.; Zhang, H. B. Carbon nanotube-supported Pd-ZnO catalyst for hydrogenation of CO_2 to methanol. *Appl. Catal., B* **2009**, *88*, 315−322.
(23) Zhang, H. B.; Liang, X. L.; Dong, X.; Li, H. Y.; Lin, G. D. Multi-walled carbon nanotubes as a novel promoter of catalysts for CO/CO_2 hydrogenation to alcohols. *Catal. Surv. Asia* **2009**, *13*, 41−58.
(24) Dong, X.; Zhang, H. B.; Lin, G. D.; Yuan, Y. Z.; Tsai, K. R. Highly active CNT-promoted Cu-ZnO−Al_2O_3 catalyst for methanol synthesis from H_2/CO/CO_2. *Catal. Lett.* **2003**, *85*, 237−246.
(25) Kong, H.; Li, H. Y.; Lin, G. D.; Zhang, H. B. Pd-decorated CNT-promoted Pd-Ga_2O_3 catalyst for hydrogenation of CO_2 to methanol. *Catal. Lett.* **2011**, *141*, 886−894.
(26) Wang, G.; Chen, L.; Sun, Y.; Wu, J.; Fu, M.; Ye, D. Carbon dioxide hydrogenation to methanol over Cu/ZrO_2/CNTs: effect of carbon surface chemistry. *RSC Adv.* **2015**, *5*, 45320−45330.
(27) Ud Din, I.; Shaharun, M. S.; Subbarao, D.; Naeem, A. Synthesis, characterization and activity pattern of carbon nanofibers based copper/zirconia catalysts for carbon dioxide hydrogenation to methanol: Influence of calcination temperature. *J. Power Sources* **2015**, *274*, 619−628.
(28) Jiménez, V.; Nieto-Márquez, A.; Díaz, J. A.; Romero, R.; Sánchez, P.; Valverde, J. L.; Romero, A. Pilot plant scale study of the influence of the operating conditions in the production of carbon nanofibers. *Ind. Eng. Chem. Res.* **2009**, *48*, 8407−8417.
(29) Díaz, J. A.; Akhavan, H.; Romero, A.; Garcia-Minguillan, A. M.; Romero, R.; Giroir-Fendler, A.; Valverde, J. L. Cobalt and iron supported on carbon nanofibers as catalysts for Fischer−Tropsch synthesis. *Fuel Process. Technol.* **2014**, *128*, 417−424.
(30) Díaz, J. A.; Martínez-Fernández, M.; Romero, A.; Valverde, J. L. Synthesis of carbon nanofibers supported cobalt catalysts for Fischer−Tropsch process. *Fuel* **2013**, *111*, 422−429.
(31) Jiménez, V.; Sánchez, P.; Panagiotopoulou, P.; Valverde, J. L.; Romero, A. Methanation of CO, CO_2 and selective methanation of CO, in mixtures of CO and CO_2, over ruthenium carbon nanofibers catalysts. *Appl. Catal., A* **2010**, *390*, 35−44.
(32) Nieto-Márquez, A.; Jiménez, V.; Raboso, A. M.; Gil, S.; Romero, A.; Valverde, J. L. Influence of the chemical activation of carbon nanofibers on their use as catalyst support. *Appl. Catal., A* **2011**, *393*, 78−87.
(33) Aksoylu, A. E.; Freitas, M. M. A.; Figueiredo, J. L. Pt-Sn catalysts supported on activated carbon. I. The effects of support modification and impregnation strategy. *Appl. Catal., A* **2000**, *192*, 29−42.
(34) Figueiredo, J. L.; Pereira, M. F. R.; Freitas, M. M. A.; Órfão, J. J. M. Modification of the surface chemistry of activated carbons. *Carbon* **1999**, *37*, 1379−1389.
(35) Xiong, H.; Moyo, M.; Rayner, M. K.; Jewell, L. L.; Billing, D. G.; Coville, N. J. Autoreduction and Catalytic Performance of a Cobalt Fischer−Tropsch Synthesis Catalyst Supported on Nitrogen-Doped Carbon Spheres. *ChemCatChem* **2010**, *2*, 514−518.
(36) Xiong, H.; Motchelaho, M. A. M.; Moyo, M.; Jewell, L. L.; Coville, N. J. Influence of supports on catalytic behavior of nickel catalysts in carbon dioxide reforming of toluene as a model compound of tar from biomass gasification. *J. Catal.* **2011**, *278*, 26−40.
(37) Díez-Ramírez, J.; Valverde, J. L.; Sánchez, P.; Dorado, F. CO_2 Hydrogenation to Methanol at Atmospheric Pressure: Influence of the Preparation Method of Pd/ZnO Catalysts. *Catal. Lett.* **2016**, *146*, 373.
(38) Leino, A. R.; Mohl, M.; Kukkola, J.; Mäki-Arvela, P.; Kokkonen, T.; Shchukarev, A.; Kordas, K. Low-temperature catalytic oxidation of multi-walled carbon nanotubes. *Carbon* **2013**, *57*, 99−107.
(39) Román-Martínez, M. C.; Cazorla-Amorós, D.; Linares-Solano, A.; de Lecea, C.S.-M. TPD and TPR characterization of carbonaceous supports and Pt/C catalysts. *Carbon* **1993**, *31*, 895−902.
(40) Nozawa, K.; Endo, N.; Kameoka, S.; Tsai, A. P.; Ishii, Y. Catalytic properties dominated by electronic structures in PdZn, NiZn, and PtZn intermetallic compounds. *J. Phys. Soc. Jpn.* **2011**, *80*, 064801.
(41) Antolini, E.; Cardellini, F. Formation of carbon supported PtRu alloys: An XRD analysis. *J. Alloys Compd.* **2001**, *315*, 118−122.
(42) Hyun, K.; Lee, J. H.; Yoon, C. W.; Kwon, Y. The effect of platinum based bimetallic electrocatalysts on oxygen reduction

DOI: 10.1021/acs.iecr.6b00170
Ind. Eng. Chem. Res. 2016, 55, 3556−3567

reaction of proton exchange membrane fuel cells. *Int. J. Electrochem. Sci.* **2013**, *8*, 11752−11767.
(43) Jacob, K. T.; Raj, S.; Rannesh, L. Vergard's law: A fundamental relation or an approximation? *Int. J. Mater. Res.* **2007**, *98*, 776−779.
(44) Gil, S.; Muñoz, L.; Sánchez-Silva, L.; Romero, A.; Valverde, J. L. Synthesis and characterization of Au supported on carbonaceous material-based catalysts for the selective oxidation of glycerol. *Chem. Eng. J.* **2011**, *172*, 418−429.
(45) Choi, S.; Park, K. H.; Lee, S.; Koh, K. H. Raman spectra of nano-structured carbon films synthesized using ammonia-containing feed gas. *J. Appl. Phys.* **2002**, *92*, 4007−4011.
(46) Dresselhaus, M. S.; Dresselhaus, R.; Saito, R.; Jorio, A. Raman spectroscopy of carbon nanotubes. *Phys. Rep.* **2005**, *409*, 47−99.
(47) Tuinstra, F.; Koenig, J. L. Raman spectrum of graphite. *J. Chem. Phys.* **1970**, *53*, 1126.
(48) Nemanich, R. J.; Solin, S. A. First- and second-order Raman scattering from finite-size crystals of graphite. *Phys. Rev. B: Condens. Matter Mater. Phys.* **1979**, *20*, 392−401.
(49) Menon, M.; Andriotis, A. N.; Froudakis, G. E. Curvature dependence of the metal catalyst atom interaction with carbon nanotubes walls. *Chem. Phys. Lett.* **2000**, *320*, 425−434.
(50) Plomp, A.; Schubert, T.; Storr, U.; de Jong, K.; Bitter, J. Reducibility of Platinum Supported on Nanostructured Carbons. *Top. Catal.* **2009**, *52*, 424−430.
(51) Chambers, A.; Nemes, T.; Rodriguez, N. M.; Baker, R. T. K. Catalytic Behavior of Graphite Nanofiber Supported Nickel Particles. 1. Comparison with Other Support Media. *J. Phys. Chem. B* **1998**, *102*, 2251−2258.
(52) Chesnokov, V. V.; Prosvirin, I. P.; Zaitseva, N. A.; Zaikovskii, V. I.; Molchanov, V. V. Effect of the Structure of Carbon Nanofibers on the State of an Active Component and on the Catalytic Properties of Pd/C Catalysts in the Selective Hydrogenation of 1,3-Butadiene. *Kinet. Catal.* **2002**, *43*, 838−846.
(53) Ochoa-Fernández, E.; Chen, D.; Yu, Z.; Tøtdal, B.; Rønning, M.; Holmen, A. Effect of carbon nanofiber-induced microstrain on the catalytic activity of Ni crystals. *Surf. Sci.* **2004**, *554*, L107−L112.
(54) Zhao, T.-J.; Chen, D.; Dai, Y.-C.; Yuan, W.-K.; Holmen, A. The effect of graphitic platelet orientation on the properties of carbon nanofiber supported Pd catalysts prepared by ion exchange. *Top. Catal.* **2007**, *45*, 87−91.
(55) Xiong, H.; Motchelaho, M. A. M.; Moyo, M.; Jewell, L. L.; Coville, N. J. Cobalt catalysts supported on a micro-coil carbon in Fischer−Tropsch synthesis: A comparison with CNTs and CNFs. *Catal. Today* **2013**, *214*, 50−60.

DOI: 10.1021/acs.iecr.6b00170
Ind. Eng. Chem. Res. 2016, 55, 3556−3567